V International Conference on Simulation for Additive Manufacturing
Sim-AM 2025
F. Auricchio, M. Carraturo and S. Morganti (Eds)

ANALYTICAL LPBF MELT POOL SIMULATION AND EXPERIMENTATION FOR METAMATERIAL LATTICES

WESSEL W. WITS[*†], CAMILL DE VOS[*] TIM KOENIS[*] AND MARC DE SMIT[*]

[*] NLR – Royal Netherlands Aerospace Centre
Metal Additive Manufacturing and Computational Mechanics
Marknesse, The Netherlands
e-mail: Wessel.Wits@nlr.nl

[†] University of Twente
Multiscale Modeling and Simulation
Enschede, The Netherlands
email: W.W.Wits@utwente.nl

Key words: Additive Manufacturing (AM), Laser Powder Bed Fusion (LPBF), Melt pool simulation, Computational modelling, Metamaterials

Abstract. This study presents an analytical model for predicting melt pool dimensions to fabricate metamaterial lattices using Laser Powder Bed Fusion (LPBF). The model considers key process parameters such as laser power and scanning speed, and relevant material properties. The model is validated for Stainless Steel 316L (SS316L) and is used to predict the processability of unsupported overhanging structures that are typically part of metamaterial lattices. Experimental results show good agreement with the model predictions and optimal LPBF process parameters are selected to fabricate high-quality metamaterial lattice structures, including auxetic structures that are capable of impact energy absorption. The model provides valuable insights into the relationships between LPBF process and material parameters, and the resulting melt pool geometry, enabling rapid prediction and optimization of process parameters.

1 INTRODUCTION

Laser Powder Bed Fusion (LPBF) has emerged as a pivotal additive manufacturing technique, enabling the fabrication of complex geometries with high precision. Metamaterial lattices, characterized by architected periodic structures, have garnered significant interest due to their unique mechanical properties and potential applications across various engineering domains [1]. However, sizing of the lattice struts requires accurate prediction of the melt pool geometry. In particular, unsupported horizontally overhanging struts, exemplary for auxetic lattice structures, are challenging to fabricate with consistent quality [2]. Traditional finite element analyses are computationally intensive and may not be practical for optimization of the LPBF process parameters. In this respect, analytical models offer a more efficient approach to predict the melt pool characteristics, yet their application to the fabrication of complex metamaterial lattices remains underexplored.

In this study, we have developed an analytical model tailored to predict the melt pool geometry and dimensions specific to the fabrication of metamaterial lattices using LPBF. The model integrates key process parameters, including laser power and scanning speed, and relevant material properties, to estimate the melt pool width, depth and length. The model is

validated for Stainless Steel 316L (SS316L) based on thin-walled structures. To predict the processability of unsupported horizontally overhanging struts, the thermal behaviour of material consolidation directly on powder is considered. Results show that in particular the melt pool depth and most significantly the length are influenced.

2 NUMERICAL MODELLING

Several analytical models have been proposed in literature to understand the solidification behaviour and dimensioning of a single laser scan track in LPBF based on the selected process parameters. These models typically compute the melt pool geometry as a starting point to predict the scan track dimensions. For instance, Tang et al. [3] have proposed a simple equation based on the Rosenthal equation, using laser power, scan speed, and material/powder bed parameters to compute the melt pool geometry. Rubenchik et al. [4] have developed a refined model using the Eagar-Tsai temperature fields model [5] and dimensionless scaling laws. Letenneur et al. [6] have validated an analytical model for SS316L in which they model laser beam energy on a semi-infinite solid representing the powder bed with a Gaussian beam assumption. Recently, Vanini et al. [7] have even developed an analytical model to predict the local material microstructure for stainless steel using a thermal field solution based on a moving Goldak heat source.

In this paper, the aforementioned models are utilised and extended specifically for modelling structures, such as unsupported horizontally overhanging struts, that are typically present in metamaterial lattices. The laser beam interacting with the powder bed is represented by a Gaussian beam model, in which the illumination time on the powder bed surface is determined by the laser scan speed and laser spot size, and the powder bed is modelled as a semi-infinite solid. The resulting temperature distribution within the powder bed, induced by the laser energy, can be described by:

$$T(x,y,z) = T_0 + \frac{A_{PB}P}{\frac{1}{2}dk_{PB}\pi^{\frac{3}{2}}} \int_{-\infty}^{0} \frac{1}{1+\tau^2} e^{-\frac{\tau^2}{1+\tau^2}\left(\left(\xi-\frac{P\acute{e}}{2\tau^2}\right)^2+\eta^2\right)-\tau^2\zeta^2} d\tau \tag{1}$$

$$\xi = 2\sqrt{2}\frac{x}{d}, \eta = 2\sqrt{2}\frac{y}{d}, \zeta = 2\sqrt{2}\frac{z}{d}, P\acute{e} = \frac{dv}{4\sqrt{2}\alpha_{PB}}, \tau = \frac{d}{4\sqrt{2\alpha_{PB}t}}$$

where, T_0 is the powder bed temperature, which was set to 150°C in this study controlled by the LPBF preheating temperature, A_{PB} is the material-specific absorptivity [-] of the laser energy by the powder bed, P is the laser power [W], d is the laser spot diameter [m], k_{PB} is the material-specific thermal conductivity of the powder bed [W/m·K], $P\acute{e}$ is the dimensionless Péclet number, representing the ratio of advective to diffusive heat transfer within the powder bed, and v is the travel speed of the melt pool [m/s], which is assumed to be equal to the laser scan speed.

The coordinate system (ξ, η, ζ) of Equation (1) is normalised to Cartesian coordinates (x, y, z) with respect to the laser spot size. Similarly, the time constant τ is normalised with respect to the thermal diffusivity, laser spot size and process time t [s].

Of particular importance for this study are the material-dependent thermal parameters. Hereto, relevant parameters are combined in the thermal diffusivity α_{PB} [m^2/s] of the powder bed, defined as:

$$\alpha_{PB} = \frac{k_{PB}}{\rho_{PB}c_{p,PB}} \tag{2}$$

where, ρ_{PB} and $c_{p,PB}$ are the powder bed density [kg/m^3] and the powder bed specific heat capacity [J/kg·K], respectively.

To predict the melt pool geometry, the computational domain is defined as follows:

- 600 µm along the laser scan direction (*x*-axis)
- 300 µm across the laser scan direction (*y*-axis)
- 100 µm powder bed thickness (*z*-axis).

Due to the Gaussian model, the temperature distribution will be symmetrical with respect to the scan direction. The coordinate system origin is centred at the laser spot targeting the top surface of the powder bed with the laser scan direction in the negative *x*-direction.

The analytical model provides tractable and computationally efficient prediction of the melt pool geometry; however, a number of complex involved physics are ignored. For instance, radiative and convective heat transfer are ignored, phase change and solidification effects from a porous medium to a solid, as well as melt pool fluidics are ignored. Hence, it is important to validate the model across a range of parameters.

To characterise the melt pool dimensions, locally computed temperatures are capped at the melting temperature of 1400°C for SS316L [6]. Temperatures above this threshold indicate a molten material state. A typical simulated melt pool geometry is illustrated in Figure 1. In this case, the laser power and scan velocity are 92 W and 370 mm/s, respectively.

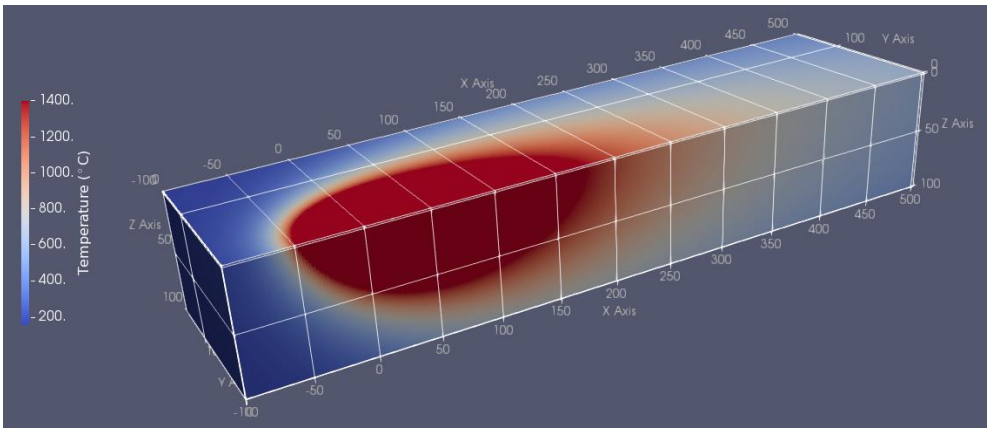

Figure 1: Simulated melt pool geometry used to predict the width of a scan track.

3 EXPERIMENTAL MODEL VALIDATION

To validate the analytical melt pool model, the width of LPBF-fabricated thin-wall structures is predicted and compared to experimental results. Single scan tracks were stacked on top of each other, hereby constructing thin walls. All experimental trials were conducted on a Nikon SLM Solution 280HL machine. The measured thin-wall widths are shown as black dots in Figure 2. The thin-wall widths were measured from a cross section and averaged along the height, as illustrated by the bottom-right inset. The grey area shows the simulated width of the melt pool. The vertical spread of the presented results is due to variations in laser power-scan speed combinations for an equal linear energy density. In addition, for the measured wall widths also process variations (i.e. noise) should be considered. The figure demonstrates that the model is well capable of predicting the width of single scan tracks, in particular if the linear energy density is higher than 0.24 J/mm.

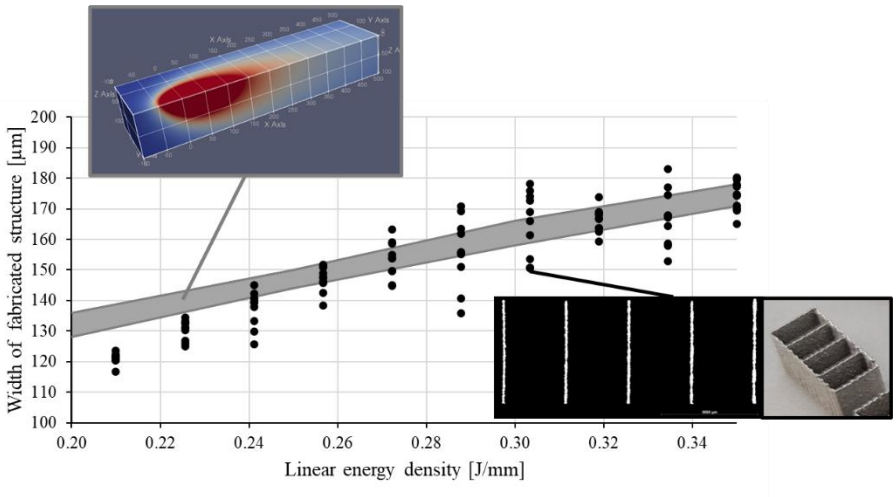

Figure 2: Simulated melt pool width (grey area) validated against experimental data (black dots); insets shown an exemplary computational results and the experimental approach.

In the case of thin-wall fabrication by LPBF, each subsequent scan track is fabricated on top of the previously consolidated track. Hence, relatively good thermal conductivity towards the build plate is present, see Figure 3(a). To predict the processability of unsupported horizontally overhanging struts of metamaterials, the thermal behaviour of consolidating directly on powder should be considered, see Figure 3(b). However, the effective powder bed thermal conductivity is significantly lower compared to solid material. In fact, Lee et al. [8,9] experimentally determined the effective powder bed thermal conductivity to be only 0.32 W/m·K, which is significantly lower than the validated thermal conductivity for the fabrication of the thin-walled structures (i.e. 23.2 W/m·K). Hence, for metamaterial lattices, the thermal conductivity towards the build plate is severely compromised and should be considered with selecting the optimal processing conditions.

Most metamaterial lattice designs contain vertical (as well as diagonal) struts. Figure 3(c) illustrates a compromise in which two parallel conductive heat flow paths towards the build plate are considered. In this case, a thermal resistance network model can be used to compute the equivalent thermal conductivity to the build plate. Following this approach, the thermal conductivity for fabricating unsupported horizontally overhanging struts is modelled to be 4.90 W/m·K; still about 5x lower compared to conventional supported LPBF fabrication strategies.

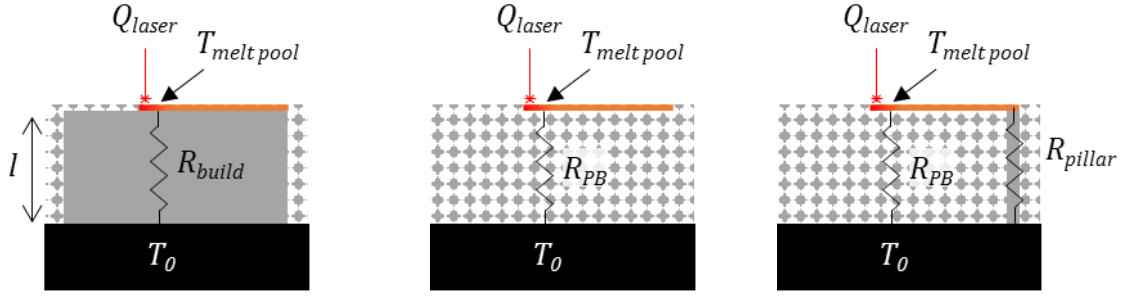

a) fabrication on consolidated powder (i.e. solid material)

b) fabrication directly on the powder bed

c) as b) but with conduction through a solid pillar as well

Figure 3: Thermal resistance model to determine thermal conductivity to the baseplate.

4 SIMULATING METAMATERIAL LATTICE STRUCTURES

Metamaterial lattices feature periodic architected structures leading to their distinctive mechanical properties. Accurate prediction of the melt pool geometry is crucial for sizing the lattice struts, particularly for unsupported overhanging struts that are commonly found in auxetic lattice structures and pose significant fabrication challenges. Using the afore adjusted thermal conductivity value, the experimentally validated analytical model is applied to predict the melt pool geometry for the fabrication of unsupported horizontally overhanging struts. Figure 4 depicts the melt pool geometry for the same processing conditions as used to predict the melt pool geometry of Figure 1. By comparing both images, it is clear that the ability of the melt pool to down towards the build plate has a tremendous influence on the melt pool geometry. When fabricating directly on powder, the poor thermal conductivity causes relatively slow cool-down rates and hence a very elongated melt pool.

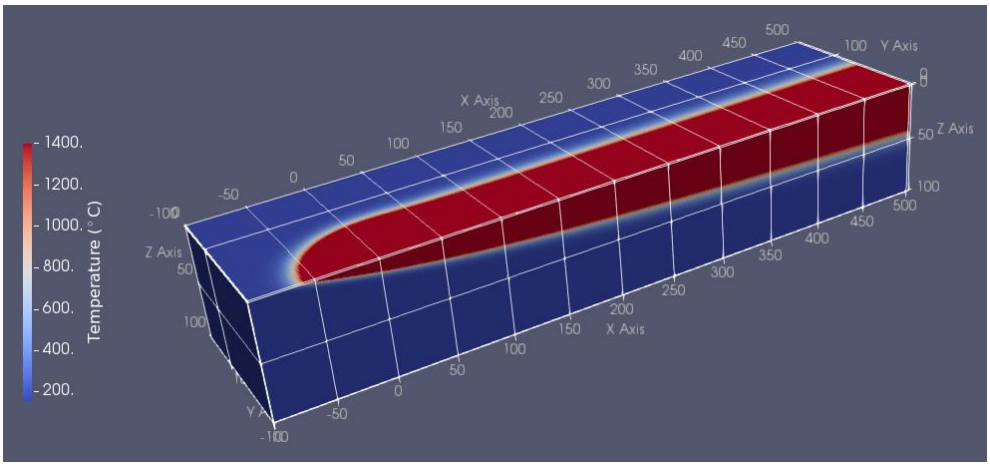

Figure 4: Melt pool geometry with adjusted thermal conductivity to simulate fabrication directly on powder.

Using the adjusted model, a new set of scan track widths is predicted and depicted in Figure 5 by the grey line; the bottom-right inset shows the simulation result at a linear energy density of 0.45 J/mm. The predicted results show that in particular the melt pool depth and most significantly the melt pool length are influenced by the lower thermal conductivity. In particular, the length is typically about 4x longer and illustrated in the figure inset. Note that in this case the computational domain was also extended in the *x*-direction. The fact that the width is less influenced, typically about 2x wider, can be attributed to the finite width of the laser spot size. The primary effect of the elongated melt pool lengths can be attributed to the adapted time constant τ in Equation (1), which has a large influence on the temperatures in the scan direction.

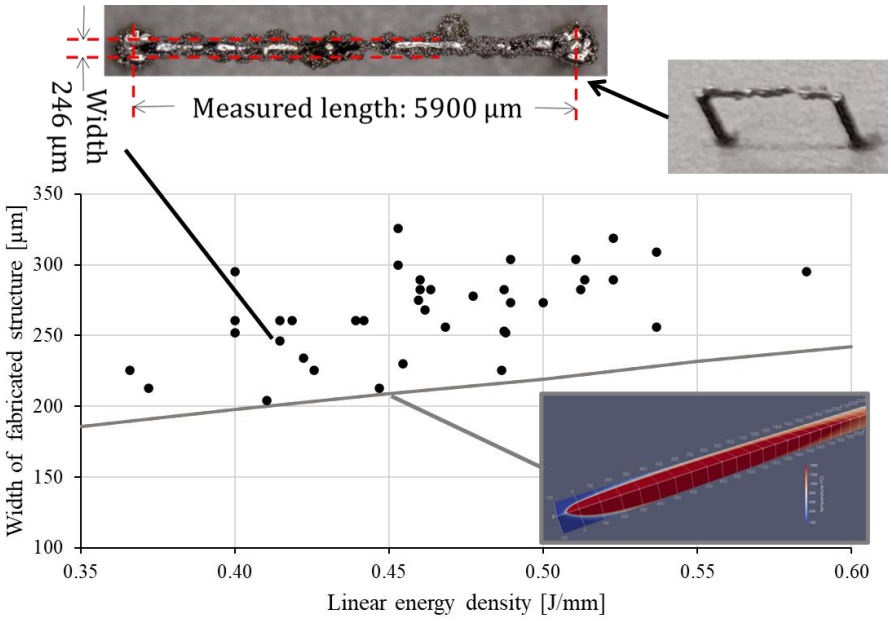

Figure 5: Simulated melt pool width (grey line) and experimental data (black dots) for overhanging structures; insets show the experimental approach and an exemplary computational results.

Figure 5 also depicts the results of a second experimental campaign in which unsupported horizontally overhanging struts were fabricated between two vertical pillars, as illustrated by the top-right inset. The widths of these struts were measured using a Keyence VHX-1000 digital light microscope and presented as black dots in the figure. The top-left inset depicts one such measurement.

The fabricated overhanging struts show a significant number of unfused powder particles due to hindered heat dissipation towards the build plate, resulting from fabrication directly on the powder bed without solid supports. This leads to high melt pool temperatures, causing lateral gas flow [10] and powder entrainment, known as the denudation process. The denudation effect contributes to the structures' increased width, approximately three times the laser spot diameter, as powder is cleared from the powder bed adjacent to the scan track and drawn into the melt pool. Additionally, the overhanging struts exhibit balling, caused by melt pool overheating [11], which induces Marangoni flow and circulatory motion. Balling is also known to occur due to poor wetting with the loose powder particles underneath the melt pool in particular at high laser scan speeds. Finally, the elongated melt pool resulting from the poor thermal dissipation may also contribute to balling due to Plateau-Rayleigh instabilities [12].

The simulation results of Figure 5 show that the predicted maximum melt pool width is limited by the laser spot size with a maximum simulated scan track width of 242 µm at the highest linear energy density of 0.60 J/mm. As aforementioned, excess energy instead causes significant melt pool elongation. Results show that the conduction-based analytical model of Equation (1) leads to underpredictions at such high melt pool temperatures. To improve the accuracy for simulating overhanging struts, the model should be extended to incorporate fluid dynamics, convective and radiative heat transfer, as well as the denudation effect, which draws additional powder particles into the melt pool making the scan track even wider.

5 METAMATERIAL FABRICATION

Based on a compromise between overhanging and inclined struts, for the fabrication of full-size metamaterial lattices a relatively low linear energy density of 0.41 J/mm is selected. In this way, an attempt was made to avoid overheating. Difficult-to-print auxetic metamaterial structures, due to horizontally unsupported struts, as well as easier-to-print octet truss structures were fabricated by LPBF. Four towers featuring an auxetic lattice structures and four towers featuring an octet truss structured were designed and fabricated using SS316L as feedstock material. The resulting successful build is shown in Figure 6(a).

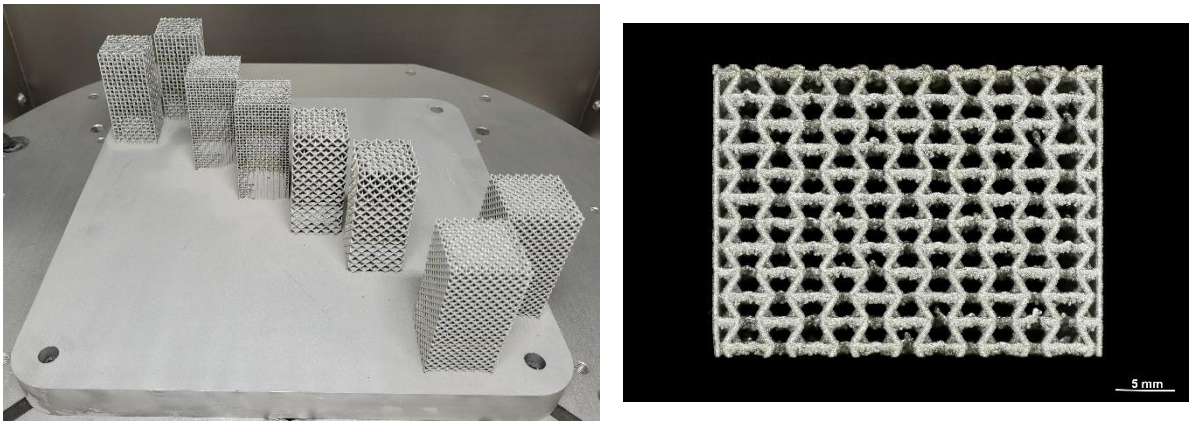

a) Fabricated baseplate with eight metamaterial towers b) Metamaterial cube wire cut from a tower

Figure 6: LPBF of full-size metamaterial lattices.

The quality of the selected LPBF parameter set can be inferred from Figure 6(b). The unsupported horizontally overhanging struts are generally well fabricated. Moreover, during impact testing of the auxetic structures using a drop-weight tester, a progressive material resistance was determined from the stress-strain measurement. The measured specific energy absorption was about 8.0-10.3 kJ/kg, which, for SS316L, is relatively high compared to other reported values [13,14].

Although the overhanging struts exhibit some defects, such as sporadic balling and loose powder attachment, the solidified lattice structures demonstrate sufficient integrity to transfer the impact loads, enabling the structure to function effectively as an auxetic metamaterial. Hence, the presence of (minor) local defects does not appear to compromise the overall mechanical behaviour of the metamaterial lattice, allowing it to exhibit the desired auxetic properties, such as negative Poisson's ratio, under the impact conditions. This suggests that the fabricated metamaterial lattice structures provide unique mechanical advantages associated to its auxetic behaviour, including efficient energy absorption and enhanced mechanical flexibility.

6 CONCLUSIONS

The presented findings provide valuable insights into the complex relationships between LPBF process parameters and resulting melt pool geometry. The models rapid predictive capabilities make it a valuable asset for selecting optimal parameters, reduce extensive empirical testing and enable the fabrication of high-quality metamaterial lattices. LPBF

experiments have been conducted, in which horizontally overhanging struts are fabricated. The experimental results show agreement with the predictions of our analytical model with deviations (i.e. underpredictions) within understandable margins. Subsequently, optimal LPBF process parameters were selected to successfully fabricate a number of metamaterial lattice structures, including difficult-to-print auxetic structures.

As a result of this study, optimal LPBF process parameters have been established for fabricating unsupported horizontally overhanging struts, a crucial component of auxetic re-entrant metamaterials. Single overhanging struts were systematically produced and their quality and size were observed by microscopic investigation. Notably, for SS316L, good processability was achieved using a higher linear energy density than is typically used in conventional process parameters. Metamaterial lattice structures were successfully fabricated using LPBF and subsequently subjected to impact testing to assess their energy absorption characteristics. The results demonstrate effective energy transfer through the metamaterial structure, as well as the manifestation of auxetic material behaviour.

These findings underscore the potential of LPBF-fabricated auxetic metamaterial lattices for applications requiring enhanced energy absorption, mechanical flexibility and/or unique mechanical properties. Furthermore, this research paves the way for the development of complex metamaterial lattice structures with tailored properties, enabling innovative solutions in various fields, such as aerospace, biomedical, and automotive engineering.

REFERENCES

[1] Wits, W. W., De Vos, C., Montero-Sistiaga, M., and De Smit, M., (2025). Laser powder bed fusion of 3D metamaterials for energy absorption. *Procedia CIRP*, vol. 137, 374-379, DOI: 10.1016/j.procir.2025.02.278.

[2] Wits W.W., De Vos, C., Montero-Sistiaga, M. and De Smit, M., (2025). Laser powder bed fusion process parameters for the fabrication of unsupported overhang structures of metamaterial lattices. *CIRP Annals - Manufacturing Technology*, vol. 71 (1), 309-313, DOI: 10.1016/j.cirp.2025.03.003.

[3] Tang, M., Pistorius, P.C. and Beuth, J.L., (2017). Prediction of lack-of-fusion porosity for powder bed fusion. *Additive Manufacturing*, vol. 14, 39-48, DOI: 10.1016/j.addma.2016.12.001.

[4] Rubenchik, A.M., King, W.E. and Wu, S.S., (2018). Scaling laws for the additive manufacturing. *Journal of Materials Processing Technology*, vol. 257, 234-243, DOI: 10.1016/j.jmatprotec.2018.02.034.

[5] Eagar, T.W. and Tsai, N.S., (1983). Temperature fields produced by traveling distributed heat sources. *Welding journal*, vol. 62 (12), 346-355.

[6] Letenneur, M., Kreitcberg, A., and Brailovski, V., (2019). Optimization of LPBF Processing Using a Combination of Melt Pool Modeling and Design of Experiment Approaches: Density Control. *Journal of Manufacturing and Materials Processing*, vol. 3(1), 21, DOI: 10.3390/jmmp3010021.

[7] Vanini, M., Searle, S., Vanmunster, L., Vanmeensel, K. and Vrancken, B., (2025). Local microstructure engineering of super duplex stainless steel via dual laser powder bed fusion–an analytical modeling and experimental approach. *Additive Manufacturing*, 104994, DOI: 10.1016/j.addma.2025.104994.

[8] Lee, H., Koutsioukis, A., Jafari, D., Geurts, B.J. and Wits, W.W., (2024). Measurement of effective thermal conductivity of composite powders of 2D materials and metals for additive manufacturing. *Journal Physics: Conference Series*, vol. 2766(1), 012186, DOI:

10.1088/1742-6596/2766/1/012186.

[9] Lee, H., Jafari, D., Koutsioukis, A., Nicolosi, V., Geurts, B.J. and Wits, W.W., (2025). Characterization of thermal properties of ball-milled copper-graphene powder as feedstock for additive manufacturing. *Powder Technology*, vol. 466, 121423, DOI: 10.1016/j.powtec.2025.121423.

[10] Matthews, M.J., Guss, G., Khairallah, S.A., Rubenchik, A.M., Depond, P.J. and King, W.E., (2016). Denudation of metal powder layers in laser powder bed fusion processes. *Acta Materialia*, vol. 114, 33-42, DOI: 10.1016/j.actamat.2016.05.017.

[11] Lindström, V., Lupo, G., Yang, J., Turlo, V. and Leinenbach, C., (2023). A simple scaling model for balling defect formation during laser powder bed fusion, *Additive Manufacturing*, vol. 63, 103431, DOI: 10.1016/j.addma.2023.103431.

[12] Zöller, C., Adams, N.A. and Adami, S., (2023). Numerical investigation of balling defects in laser-based powder bed fusion of metals with Inconel 718, *Additive Manufacturing*, vol. 73, 103658, DOI: 10.1016/j.addma.2023.103658.

[13] Zhang, P., Yu, P., Zhang, R., Chen, X. and Tan, H., (2023). Grid octet truss lattice materials for energy absorption. *International Journal of Mechanical Sciences*, vol. 259, 108616, DOI: 10.1016/j.ijmecsci.2023.108616.

[14] Li, Y., Jiang, D., Zhao, R., Wang, X., Wang, L. and Zhang, L.-C., (2024). High Mechanical Performance of Lattice Structures Fabricated by Additive Manufacturing, *Metals*, vol. 14(10), 10, DOI: 10.3390/met14101165.